

Platform for JFET-based Sensing of RF MEMS Resonators in CMOS Technology

Eugene Hwang¹, Andrew Driscoll², and Sunil A. Bhave¹

¹OxideMEMS Lab, Cornell University, Ithaca, NY, USA

²United States Army

Abstract

This paper presents an RF MEMS resonator with embedded junction field effect transistor (JFET) for efficient electrical detection of the high quality factor acoustic resonance. A homogenous single-crystal silicon resonator is excited in its fundamental thickness extensional resonant mode at 1.61 GHz with a quality factor of 25,900. This device can be fully integrated into a typical SOI CMOS technology with minimal modifications to the existing front-end process. Furthermore, it achieves an acoustic transconductance of 171 μS at a bias current of 143 μA , approaching a practical range for monolithic, low-power RF systems.

Introduction

High quality factor (Q), electrostatically actuated RF MEMS resonators [1], [2] have gained the attention of RF designers for use in applications that require extreme scaling of size, weight, and power consumption. This is due to a number of advantages, including the possibility of extremely high Q resonators monolithically integrated into a foundry CMOS process. There are, however, a number of drawbacks associated with electrostatic transduction of MEMS resonators, the most significant of these being the low electromechanical transduction efficiency. This results in large motional impedances, which make such devices very sensitive to parasitics, especially the parasitic feedthrough formed by the large transduction capacitances. This limits the utility of conventional electrostatic transduction to frequencies below a few hundred MHz.

To address this problem, recent work has focused on breaking the parasitic feedthrough path by using FET-based piezoresistive detection of the output signal [3]-[5]. In [3] and [4], however, the process limitations associated with creating very narrow air-gaps means that large bias voltages ($> 10\text{ V}$) are necessary for efficient actuation, especially at frequencies above 100 MHz. A method of efficient electromechanical transduction at high frequencies using an embedded solid dielectric transducer has been developed in [6], while replacing this with a pn-diode transducer has been demonstrated in [7] to retain the high Q of a single-crystal silicon structure.

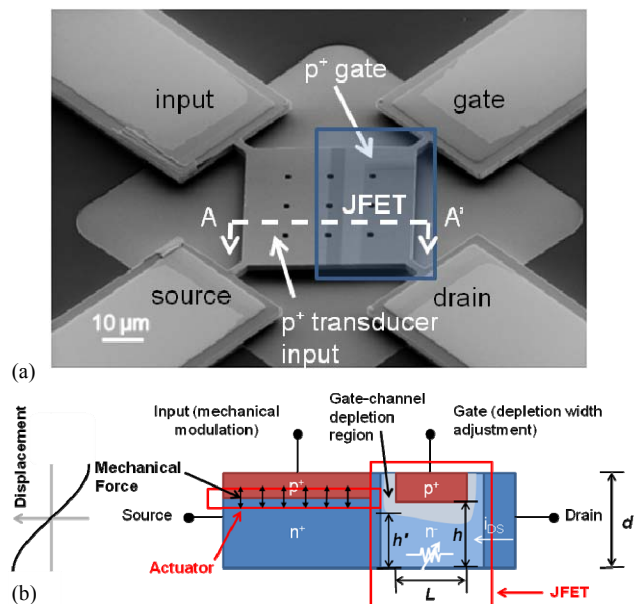


Fig. 1. (a) SEM with all four terminals labeled. Lightly contrasted regions denote areas of p-type doping. (b) Cross-section (A-A') of resonant JFET showing the actuation junction on the left and the JFET sensing element on the right. Induced resonant mechanical displacement is shown on the left.

This work combines the benefits of pn-diode actuation of a single-crystal silicon resonator with an embedded junction field effect transistor (JFET) to control the bias current for piezoresistive detection. Use of a JFET sensing element allows the structure to remain homogeneous in composition for high Q , while providing additional benefits such as lower channel and $1/f$ noise compared to MOSFETs. In addition, surface scattering of carriers in MOSFET channels is not present in bulk silicon, making the piezoresistive modulation larger in JFETs. This results in an acoustic transconductance to bias current ratio – a critical parameter for low power RF design – greater than 1 for such resonant transistors. Furthermore, the process flow can readily be integrated into a SOI CMOS technology with no changes to the front end process [8], highlighting the possibility of monolithic integration of RF MEMS resonators and CMOS in a foundry process for low-power, single-chip RF solutions.

Device Structure and Principle of Operation

Fig. 1(a) shows an SEM image of the RF MEMS resonator with embedded JFET. This device has four terminals: the

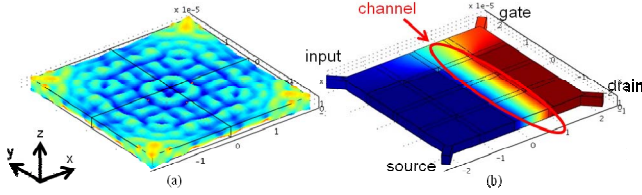


Fig. 2. (a) COMSOL simulation results of the fundamental thickness extensional mode shape highlighting the z -displacement. Irregularities in mode shape are due to etch holes. (b) Voltage distribution between source and drain contacts indicating that current flow is confined to channel placed at location of maximum displacement.

actuator input and the gate, source, and drain terminals of the JFET. A clear contrast can be seen between the lightly shaded p^+ gate and actuator inputs and the darker n^+ source and drain regions. The source terminal serves as both the JFET source and the cathode of the pn-diode actuator and thus lies underneath the p^+ actuator input on the structure. This is illustrated in the cartoon of the device cross-section shown in Fig. 1(b). On the left side of the structure is the pn-diode actuator, configured to excite the fundamental thickness extensional resonant mode (Fig. 2(a)). The displacement amplitude at resonance excited by the pn-diode actuator is [7]

$$|U_o| = \frac{2Qd^2}{n^3\pi^3 E} \frac{eN_a}{z_{d0,a}} \sin\left(\frac{n\pi d_a}{d}\right) \sin^2\left(\frac{n\pi}{d} \frac{z_{d0,a}}{2}\right) v_{in}. \quad (1)$$

Here, d is the resonator thickness, d_a is the actuator junction depth, E is the Young's modulus, n is the harmonic number, e is the elementary charge, N_a is the symmetric doping concentration, and $2z_{d0,a}$ is the total depletion width of the actuator junction. The two sinusoidal terms in (1) indicate the optimal junction placement at a displacement node and the favorable frequency scaling that are characteristics of pn-diode transduction. On the right side of the structure is the JFET used to control the bias current for piezoresistive detection of the resonant motion. The main piezoresistive contribution to the output signal is through the lightly n-doped JFET channel (Fig. 2(b)). The acoustic strain excited by the pn-diode actuator causes a modulation of the channel resistance, which appears as a motional current

$$i_{out} = 2\pi_{12} E \frac{U_o}{h'} \sin^2\left(\frac{n\pi}{d} \frac{h'}{2}\right) I_{Dsat}. \quad (2)$$

Here, I_{Dsat} is the saturation current controlled by the JFET and h' is the thickness of the JFET channel at the source, as seen in Fig. 1(b). The channel orientation is in the (100)-direction to maximize the piezoresistive response due to the strain oriented in the (001)-direction [9]. The relevant piezoresistive coefficient in this case is π_{12} as seen in (3). The saturation current of the JFET is given by [10]

$$I_{Dsat} = I_P \left[\frac{1}{3} - \frac{V_{GS} + \phi_{bi,ch}}{V_P} + \frac{2}{3} \left(\frac{V_{GS} + \phi_{bi,ch}}{V_P} \right)^{3/2} \right]. \quad (3)$$

Here, $\phi_{bi,ch}$ is the built-in voltage of the gate-channel junction of the JFET. I_P and V_P are given by

$$I_P = \frac{\mu_n e^2 N_{ch}^2 h^3}{2\epsilon_{si} \epsilon_0} \frac{W}{L_{ch}}, \quad V_P = \frac{e N_{ch} h^2}{2\epsilon_{si} \epsilon_0} \quad (4)$$

where μ_n is the electron mobility, h is the as-fabricated channel thickness (different from h' , see Fig. 1(b)), and W and L_{ch} are the device width and channel length, respectively. Eq. (4) is valid for $V_{DS} > V_P - \phi_{bi,ch} - V_{GS}$. From (2)-(4), it is evident that increasing the motional current can be achieved by increasing N_{ch} and h . Of course, these parameters should not be so large such that the channel cannot be pinched off.

To model the behavior of this device, an equivalent circuit model can be developed, as shown in Fig. 3. This equivalent circuit model is very similar to the small signal model of a typical JFET. There are two additional elements to model the acoustic resonance excited by the pn-diode actuator: a third-order resonant circuit between the input and the source node and an additional voltage controlled current source between the source and drain. The former is often seen in modeling the electromechanical resonance of typical MEMS resonators. The latter describes the motional current flowing through the drain due to the acoustic transconductance g_a given by

$$g_a = \frac{4\pi_{12} E}{h'} \sin^2\left(\frac{n\pi}{d} \frac{h'}{2}\right) I_{Dsat} \times \frac{d^2}{n^3\pi^3 E} \frac{eN_a}{z_{d0,a}} \sin\left(\frac{n\pi d_a}{d}\right) \sin^2\left(\frac{n\pi}{d} \frac{z_{d0,a}}{2}\right). \quad (5)$$

Note that the control voltage for this dependent current source is not the input voltage but rather the voltage across the capacitor in the series RLC circuit v_C . Using this definition implicitly includes the resonant behavior since the voltage across the capacitor at resonance is amplified by Q and phase shifted by 90 degrees. Also note that the motional current appears in parallel with the electrical response of the JFET transconductance. To avoid overwhelming the acoustic resonant signal, the gate is AC grounded during resonant sensing operation. It is also very important to minimize any source resistance R_s to minimize this parasitic electrical signal.

Fabrication

A simplified process flow is shown in Fig. 4. We start with an undoped, 2.5 μm device layer SOI wafer. A blanket

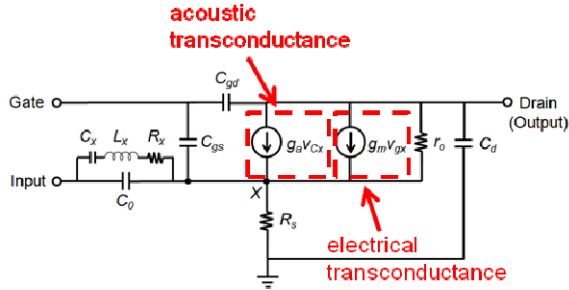


Fig. 3. Equivalent circuit model for the pn-diode actuated resonant JFET.

phosphorus implant and subsequent anneal is performed to achieve the desired channel doping. Next, a phosphorus diffusion with oxide mask is performed to selectively dope the source and drain regions of the JFETs. A boron implant and subsequent rapid thermal anneal is then performed to simultaneously define the JFET gate and pn-diode actuator. Molybdenum silicide is then sputter deposited and patterned via lift-off to form the interconnect structures. This is followed by a reactive ion etch of the device layer to define the resonator structure. Finally, a timed HF etch is used to undercut the buried oxide layer and release the structure for free mechanical motion.

Experimental Setup and Results

The experimental setup for DC characterization is shown in Fig. 5(a). A Keithley 4200-SCS parametric analyzer is used to take I-V measurements of the embedded JFET. The source terminal is grounded through GSG probes. DC measurement results are shown in Fig. 6. Fig. 6(a) shows the measured I_D - V_D characteristics of the device with -0.25 V gate bias steps from 0 to -1 V along with predictions using analytical expressions found in [10]. Agreement between measured results and analytical predictions is within 10% using $h = 0.78 \mu\text{m}$, $N_{ch} = 5.4 \times 10^{15} \text{ cm}^{-3}$, and a field-dependent mobility

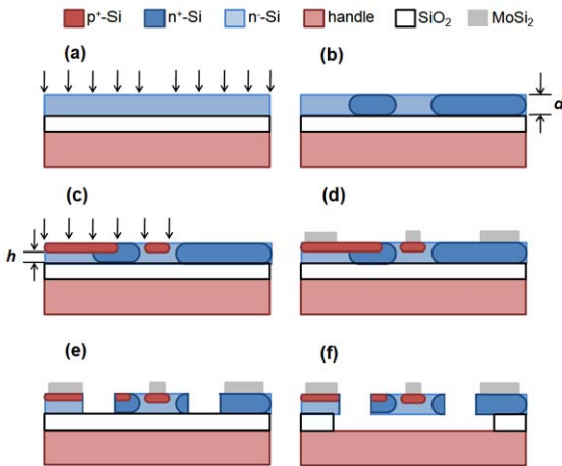


Fig. 4. Fabrication process flow for the pn-diode actuated resonant JFET.

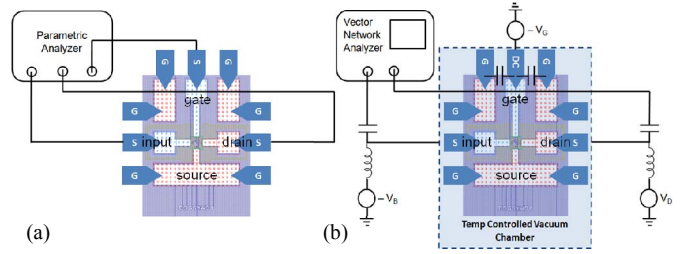


Fig. 5. Measurement setup for (a) JFET DC and (b) two-port RF measurements.

model. The saturation output resistance r_o is found to be roughly 80 k Ω . Fig. 6(b) shows the I_D - V_G characteristics of the device with 1 V drain bias steps from 1 to 4 V. This plot shows that for $V_G < -1.375$ at $V_D = 4$ V, the drain current increases. This is due to reverse breakdown of the gate-drain junction resulting in addition drain current that flows to the gate rather than through the channel to the source.

Fig. 5(b) shows the RF measurement setup to characterize the acoustic resonance of the device. A vector network analyzer is used to obtain S-parameter measurements, which can then be converted to acoustic transconductance using the expression $g_a = Y_{21} - Y_{12}$. The JFET gate is biased through a controlled impedance DC probe with AC coupling capacitors to ground placed at the probe tip. Input actuator and drain biases are applied through bias-Ts. Measurements are taken with the device in a temperature controlled vacuum chamber. Fig. 7(a) shows the acoustic transconductance as a function of frequency, showing a clear resonant peak at roughly 1.61 GHz with a maximum value of 171 μS . This value is obtained with $V_G = -0.3\text{V}$ and $V_D = 2.8$ V for a bias current of 143 μA and an actuator bias of $V_B = -5$ V, yielding $g_a/I_D = 1.2$. Changing V_B to -4 V shows a distinct change in the resonant frequency and the acoustic transconductance, verifying that this resonant peak is due to acoustic resonance excited by the pn-diode actuator. The Q obtained for this resonator at room temperature is 25,900, which results in an f - Q product of 4.17×10^{13} Hz. Temperature measurements from -55 to 125 $^\circ\text{C}$ were also conducted and experimental resonant frequency shifts are shown in Fig. 7(b). This plot indicates that the resonant frequency linearly decreases with temperature with a temperature coefficient equal to -11.2 ppm/ $^\circ\text{C}$. This TCF is smaller than typical silicon RF MEMS resonators by a factor of 3, which is consistent with [7] and explained by degenerate doping effects [11].

Conclusions

We have presented a novel micromechanical resonator using JFET-based sensing of a pn-diode actuated RF MEMS resonator to reduce the problematic parasitic feedthrough

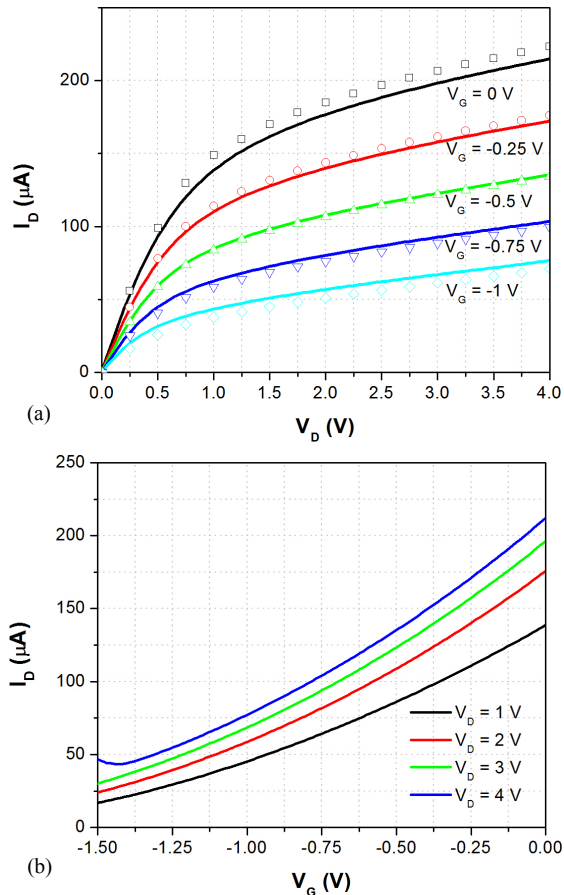


Fig. 6. (a) Measured (solid) and predicted (symbols) I_D vs. V_D characteristics of embedded JFET at different gate biases showing clear saturation behavior at large drain voltage. (b) Measured I_D vs. V_G characteristics of embedded JFET at different drain biases.

current. The acoustic transconductance to bias current ratio achieved using this device is 1.2 at a frequency of 1.61 GHz with a Q of 25,900, resulting in an f - Q product of 4.17×10^{13} Hz. Most significantly, this process can be fabricated using the front-end process flow of an existing foundry SOI CMOS process that has already demonstrated integrated Si MESFETs [8], which are very similar in structure and operation to JFETs. Such high-level integration may eventually allow for truly monolithic, low-power RF systems.

Acknowledgements

The authors would like to acknowledge the DARPA/MTO HI-MEMS program and the SRC for their generous support and the staff of the Cornell Nanoscale Science and Technology Facility (CNF) for help with device fabrication.

References

[1] S. Pourkamali *et al.*, "Low-impedance VHF and UHF capacitive silicon bulk acoustic-wave resonators – part II: Measurement and characterization," *IEEE Trans. Elec. Dev.*, vol. 54, pp. 2024-2030, August 2007.

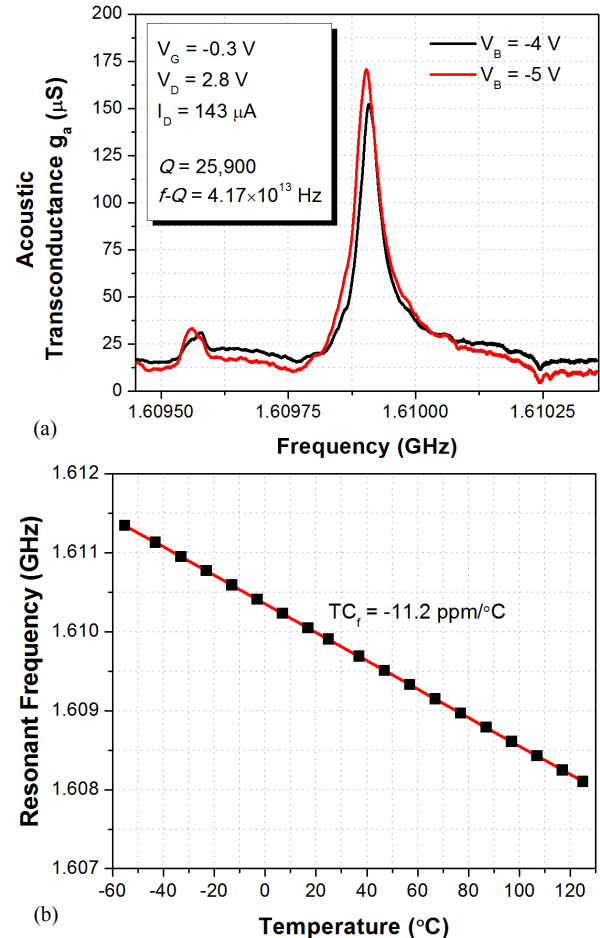


Fig. 7. (a) Measured acoustic transconductance showing clear resonant peak with $Q = 25,900$ at approximately 1.61 GHz, showing clear dependence on actuator bias voltage V_B . (b) Measured resonant frequency as a function of temperature from -55 to 125°C .

[2] C. T.-C. Nguyen, "MEMS technology for timing and frequency control," *IEEE Trans. Ultrasonics, Ferroelectrics, and Freq. Control*, vol. 54, pp. 251-270, February 2007.

[3] D. Grogg *et al.*, "Multi-gate vibrating-body field effect transistor (VB-FETs)," *IEDM 2008*, pp 663-666.

[4] Y. Xu *et al.*, "Radio frequency electrical transduction of graphene mechanical resonators," *Appl. Phys. Lett.*, 97, 243111, 2010.

[5] D. Weinstein and S. A. Bhawe, "The resonant body transistor," *Nano Letters*, vol. 10, pp. 1234-1237, 2010.

[6] D. Weinstein and S. A. Bhawe, "Internal dielectric transduction of a 4.5 GHz silicon bar resonator," *IEDM 2007*, pp. 415-418.

[7] E. Hwang and S. A. Bhawe, "PN-diode transduced 3.7 GHz silicon resonator," *IEEE MEMS 2010*, pp. 208-211.

[8] J. Ervin *et al.*, "CMOS-compatible SOI MESFETs with high breakdown voltage," *IEEE Trans. Electron Devices*, vol. 53, pp. 3129-3135.

[9] Y. Kanda, "A graphical representation of the piezoresistance coefficients in silicon," *IEEE Trans. Electron Devices*, vol. 29, pp. 64-70, 1982.

[10] S. M. Sze, *Semiconductor Devices: Physics and Technology*, 2nd Ed., New York: John Wiley & Sons, Inc., 2002, pp. 237-246.

[11] A. K. Samarao and F. Ayazi, "Temperature compensation of silicon micromechanical resonators via degenerate doping," *IEDM 2009*, pp. 789-792.